Available online at www.sciencedirect.com

ScienceDirect

Ceramics International 40 (2014) 14447–14452

CERAMICS INTERNATIONAL

www.elsevier.com/locate/ceramint

AlN powder synthesis by sodium fluoride-assisted carbothermal combustion

Haoyang Wu[a], Mingli Qin[a,*], Aimin Chu[b], Qi Wan[a], Zhiqin Cao[a,c], Ye Liu[a], Xuanhui Qu[a], Alex A. Volinsky[d]

[a]*School of Materials Science and Engineering, University of Science and Technology Beijing, Beijing 100083, China*
[b]*School of Electro-mechanism Engineering, Hunan University of Science and Technology, Xiangtan 411201, China*
[c]*School of Resources and Environmental Engineering, Pan Zhihua University, Pan Zhihua 617000, China*
[d]*Department of Mechanical Engineering, University of South Florida, Tampa FL 33620,USA*

Received 21 May 2014; received in revised form 1 July 2014; accepted 2 July 2014
Available online 10 July 2014

Abstract

AlN powders were prepared by combining sodium fluoride-assisted solution combustion with carbothermal reduction-nitridation. The effects of sodium fluoride on the nitridation reactivity, specific surface areas and morphology of the synthesized AlN powders were investigated in detail. The morphology of the AlN products changed from highly fluffy and porous networks into regular and hexagonal thin flakes, and the specific surface area decreased with the sodium fluoride content. No hard agglomeration could be found in decarburized AlN powders. The phase-pure AlN has been observed in all products calcined above 1300 °C, and no sodium was detected in the AlN powders by the X-ray fluorescence spectrometry.

Keywords: AlN powders; Sodium fluoride; Solution combustion synthesis; Carbothermal combustion

1. Introduction

Recently, aluminum nitride (AlN) ceramics have attracted considerable attention for its applications as advanced electronic substrates, heat sinks, and packaging materials, because of the high thermal conductivity ($320\ \mathrm{W\,m^{-1}\,K^{-1}}$ theoretical value), high electrical resistivity ($>10^{16}\ \Omega\mathrm{m}$), low dielectric constant (8.8 at 1 MHz), low dielectric loss (3–10 at 1 MHz), and low thermal expansion coefficient ($4.6\times10^{-6}\ \mathrm{K^{-1}}$ at 20–500 °C), closely matching silicon [1,2]. During the past few years, various techniques, including direct nitridation [3], carbothermal reduction nitridation [4–6], and chemical vapor deposition [7], have been employed to fabricate AlN. Among the available chemical processes, a carbothermal reduction-nitridation (CRN) method can yield the AlN powders with high purity, high sinterability, and stability against humidity, compared with other techniques [8]. Nevertheless, this method has also displayed some limitations, such as difficulty in homogeneously mixing the starting materials, the high cost due to the high calcination temperature, and the requirement of high purity Al_2O_3 and carbon black for the fabrication of highly pure AlN powders [9–10]. Several investigations have tried to address these issues. It has been reported that the proper selection of raw materials and the preparation of a homogeneous mixture of (Al_2O_3+C) precursors have become two essential tasks to synthesize fine AlN powders by a CRN method [11–15].

It is well known that solution combustion synthesis (SCS) is one of the proper methods to prepare materials, which exhibit well-defined chemical composition with homogeneous distribution of the elements [16]. Besides, the SCS method can save energy, rendering simple and instantaneous combustion reaction [17]. Qin et al. [4,8–9,18–20] successfully synthesized non-oxide ceramic powders by the combination of SCS and CRN. Generally, sodium fluoride has been used as an additive during SCS, to tune the combustion behavior, microstructure, and the product properties. Wen et al. [21] have first reported

---

[*] Corresponding author. Tel.: +86 10 82377286; fax: +86 10 62334311.
E-mail address: qinml@mater.ustb.edu.cn (M. Qin).

http://dx.doi.org/10.1016/j.ceramint.2014.07.014
0272-8842/

that a new type of eruption combustion in SCS by the additive of sodium fluoride, and the addition of sodium fluoride into the SCS resulted in smaller particles, improved dispersity and significantly increased specific surface area. Manjunatha et al. [22] found that the addition of 2 wt% sodium fluoride during the preparation of Sm^{3+} doped $CdSiO_3$ is highly useful in enhancing its crystallinity, morphology and thermoluminescence intensity. Inspired by these results, this paper wanted to study the effect of sodium fluoride on the nitridation reactivity, specific surface areas and morphology of the AlN powders synthesized by combining sodium fluoride -assisted SCS and CRN methods.

In the present work, sodium fluoride as an additive, aluminum nitrate as an oxidizer and aluminum source and urea as fuel, and glucose as carbon source have been utilized. AlN powders have been synthesized successfully by combining salt-assisted SCS and CRN methods. The effects of sodium fluoride on the particle sizes, phases and morphology of the precursors, along with the synthesized AlN powders have been studied in detail.

2. Experimental procedure

2.1. Starting materials

All starting materials, including aluminum nitrate ($Al(NO_3)_3 \cdot 9H_2O$, oxidizer and Al source), urea ($CO(NH_2)_2$, fuel), sodium fluoride (NaF, additive), and glucose ($C_6H_{12}O_6 \cdot H_2O$, C source) were of analytical reagent grade. The starting solution was prepared by dissolving all materials in 180 mL of distilled water. In the solution, the amount of aluminum nitrate was 0.1 M, and the molar ratio of urea to aluminum nitrate (U/Al) was 1, and the mixing molar ratio of glucose to aluminum nitrate (C/Al) was 12. The molar ratio of sodium fluoride to aluminum nitrate, denoted as φ, was in the 0–1.5 range.

2.2. Synthesis procedure

Each type of solution was filled into a 1000 mL beaker, and subsequently heated in air on an electrical temperature-controlled furnace to prepare the precursors. The electrical furnace could be heated up to 350 °C at 20 K min^{-1} heating rate. As heating continued, the solution evaporated and formed a gelatinous mass. Upon further heating, the resultant mass suddenly swelled, coupled with the release of a lot of gases. The whole process of swelling and combustion of gel seemed to undergo a self-propagating and non-explosive exothermic reaction, and lasted for several minutes, resulting in a fragile and foamy mass of precursors. The nitridation reaction of precursors was performed in a tube furnace. A strict temperature program was followed in all runs, with a constant heating rate of 10 K min^{-1} in the 1200–1500 °C range. The precursors were heated in a flowing nitrogen gas with the flow rate of 1 L min^{-1} at various temperatures for 2 h. The residual carbon in the nitridation product was removed by calcination at 700 °C in air for 2 h.

2.3. Characterization

Phases of the precursors and the nitridation products were investigated by X-ray diffraction (XRD, MXP21VAHF) at room temperature. The 2θ angle was varied from 10° to 90° in 0.02° increments. Morphology of the precursors and nitridation products was characterized by scanning electron microscopy (SEM, JSM-6510) and field emission scanning electron microscopy (FE-SEM, ZEISS ULTRA 55). The specific surface area (SSA) of the precursors and nitridation products was determined by a Brunauer–Emmett–Teller (BET) method using an automated surface area and a pore size analyzer (QUADRASORB SI-MP). The elemental analysis of the AlN powders was determined by X-ray fluorescence spectrometer (XRF, XRF-1800).

3. Results and discussion

3.1. Characterization of the precursors

Fig. 1 shows the SEM images of four precursors. Fig. 1a shows typical morphology derived by the conventional SCS ($\varphi=0$, no salt), which illustrates flakes with an average thickness of 0.3–0.6 μm. The flakes have a smooth surface. With the addition of a certain amount of sodium fluoride into the precursor solution ($\varphi=0.5$), the precursor exhibits more attenuated flaky appearance with an average thickness of 0.4–0.5 μm (Fig. 1b). For the precursors ($\varphi=1$ and 1.5), the morphology changes into porous mass (Fig. 1c and d). The SSAs of the four precursors are calculated to be 6.1, 7.6, 13.7 and 11.2 m^2 g^{-1}, respectively. It is distinct that sodium fluoride has great influence on the morphology of the precursors, and the SSA increases with the sodium fluoride additive amount, which is consistent with the phenomenon reported in the literature [21].

Figs. 2 and 3 show the XRD patterns and energy dispersive spectra (EDS) analysis of the four precursors. Fig. 2 reveals that no obvious Bragg diffraction peaks can be detected in the two precursors ($\varphi=0$ and 0.5), indicating that the two precursors are amorphous. Combining the XRD results (Fig. 2a and b) with the EDS results (Fig. 3a and b), the main compositions of the precursors ($\varphi=0$ and 0.5) are amorphous carbon and amorphous alumina (Al_2O_3+C) [8]. Comparing the two precursors ($\varphi=0$ and 0.5) reveals that there are byproducts indexed to $NaNO_3$, except for the amorphous carbon and amorphous alumina (Al_2O_3+C) in other precursors ($\varphi=1$ and 1.5). A similar phenomenon has been reported in the literature [21]. Four precursors were used to synthesize AlN powders by the CRN method in the subsequent experiments.

3.2. Nitridation reactivities of the precursors

Fig. 4 shows the XRD patterns of the four products calcined at 1200–1500 °C. No diffraction peaks can be found for the sample ($\varphi=0$) calcined at 1200 °C. It implies that the crystallization process and the nitridation reaction of the precursors

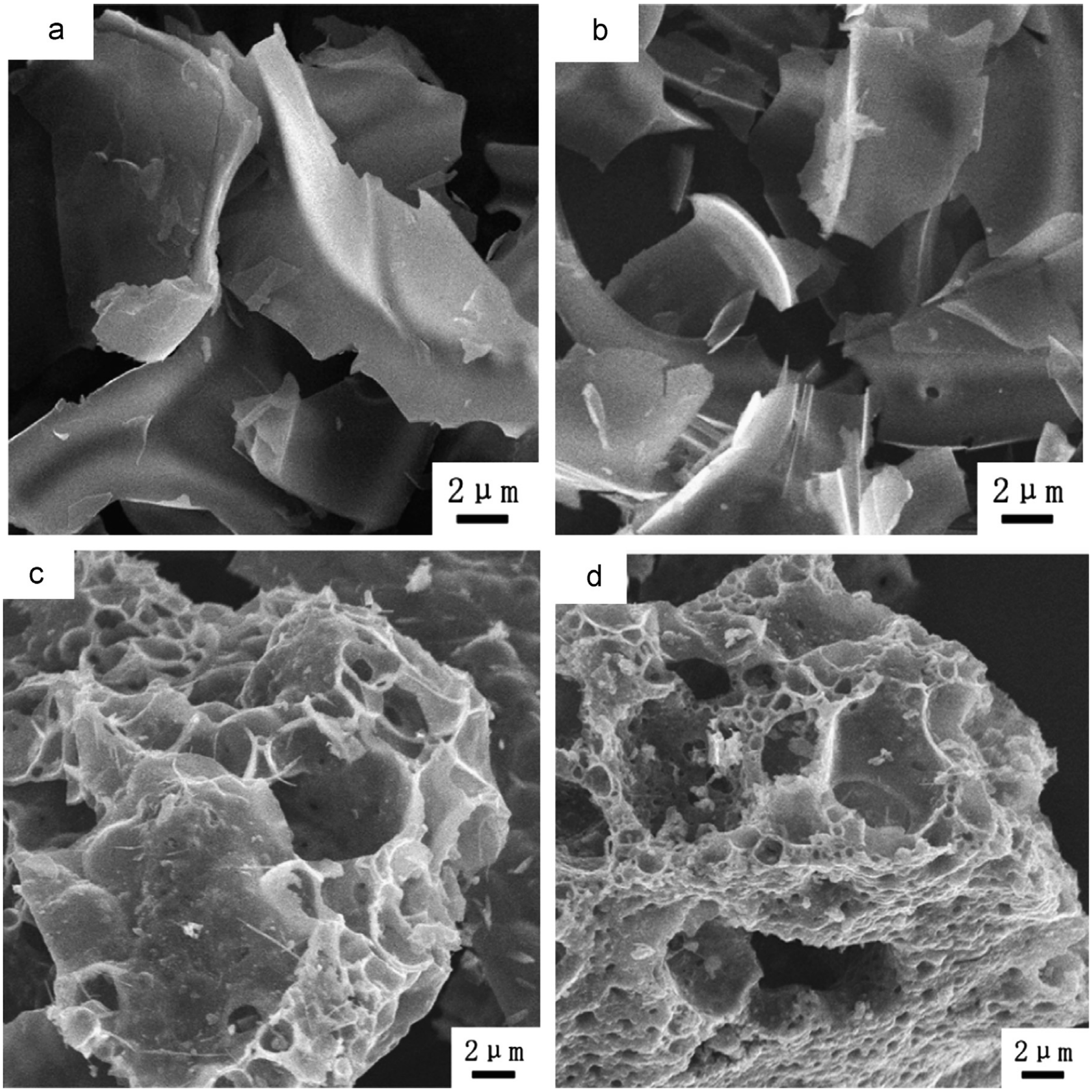

Fig. 1. SEM micrographs of precursors: (a) $\varphi=0$; (b) $\varphi=0.5$; (c) $\varphi=1$; and (d) $\varphi=1.5$.

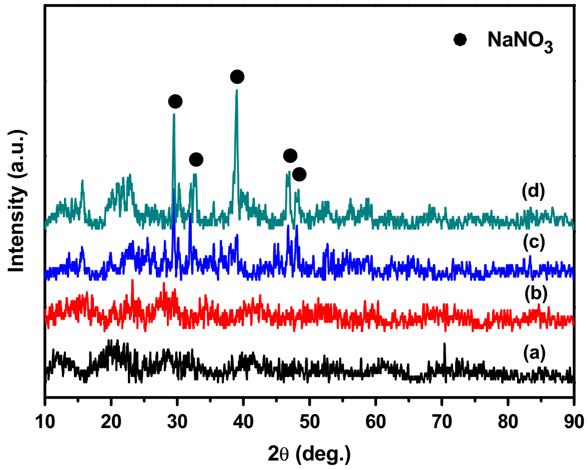

Fig. 2. XRD patterns of four precursors: (a) $\varphi=0$; (b) $\varphi=0.5$; (c) $\varphi=1$; and (d) $\varphi=1.5$.

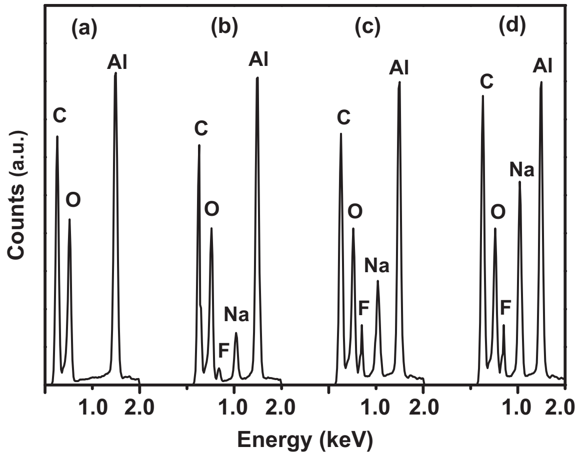

Fig. 3. EDS spectra of four precursors: (a) $\varphi=0$; (b) $\varphi=0.5$; (c) $\varphi=1$; and (d) $\varphi=1.5$.

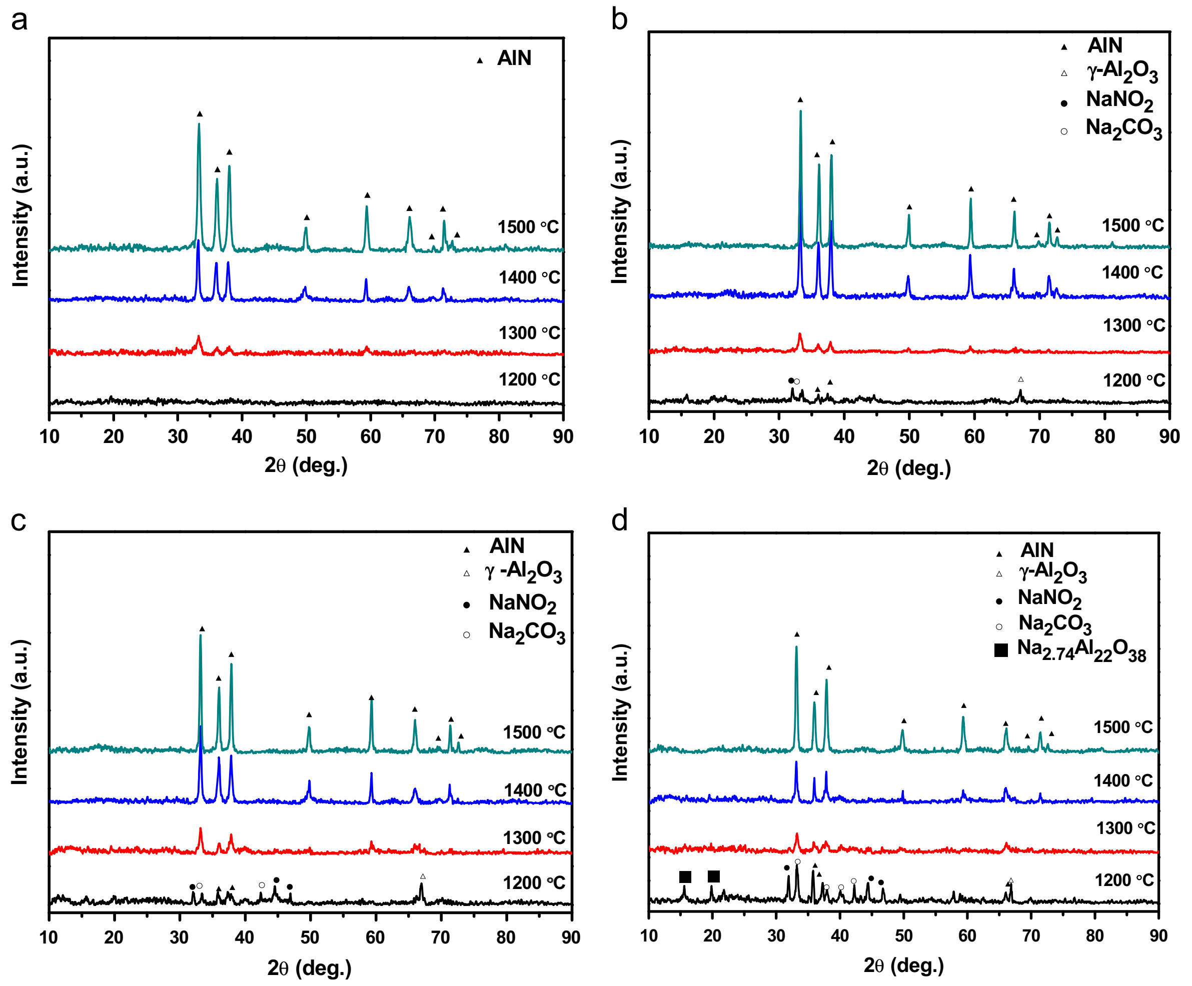

Fig. 4. XRD patterns of products calcined at various temperatures: (a) $\varphi=0$; (b) $\varphi=0.5$; (c) $\varphi=1$; and (d) $\varphi=1.5$.

have not occurred at this temperature. However, the three samples ($\varphi=0.5$, 1 and 1.5), calcined at 1200 °C, have exhibited weak diffraction peaks of Al_2O_3 and AlN, indicating crystallization process from the amorphous phase to alumina and nitridation reactivity during calcination. It can be concluded that the onset temperature of the nitridation reactions of the three precursors ($\varphi=0.5$, 1 and 1.5) is lower than that of the other precursor without the salt ($\varphi=0$). Except for the high SSA and high activity of the precursors [8], it is obvious that the molten salt would play an important role in the lower onset temperature, for the calcination temperature is higher than the melting point of the sodium salts. For samples ($\varphi=0.5$, 1 and 1.5) calcined at 1200 °C, there are byproducts indexed to $NaNO_2$, Na_2CO_3 and $Na_{2.74}Al_{22}O_{38}$, and these impurity peaks disappear above 1300 °C, ascribed to the byproducts gasification. The phase-pure AlN has been observed in all products calcined at 1300 °C, 1400 °C, and 1500 °C. To further discuss the residual sodium impurity level, AlN powders calcined at 1500 °C have been measured by XRF, and the results reveal that no sodium can be detected in AlN powders ($\varphi=0.5$, 1.0 and 1.5). This implies that the introduction of sodium fluoride into the solution combustion synthesis would not affect the purity of AlN powders.

3.3. Nitridation products microstructure

Fig. 5 shows FESEM images of the four decarburized products synthesized at 1500 °C. The product ($\varphi=0$, no salt) is composed of irregular three-dimensional flakes consisting of agglomerated particles ranging from 80 to 100 nm (Fig. 5a), which still holds the appearance of the original precursor. The average thickness of the flakes is ~0.3 μm (Fig. 5a). The effect of sodium fluoride on both morphology and particle size can be seen in Fig. 5b–d. It is obvious that the sodium fluoride plays an important role in changing the microstructure of the samples. With the addition of sodium fluoride ($\varphi=0.5$), the three-dimensional flake structure is broken up and switches to highly fluffy and porous networks consisting of spherical particles, ranging from 150 to 200 nm, as seen in Fig. 5b. For ($\varphi=1$) samples, the products are composed of irregular and thin flakes (Fig. 5c). As the sodium fluoride content is further increased ($\varphi=1.5$), the product exhibits regular hexagon morphology (Fig. 5d). Moreover, the flakes ($\varphi=1$ and 1.5) consist of irregular particles ranging from 150 to 200 nm, and their average thickness is ~100 nm (Fig. 5c and d), which is much thinner than those without the salt, at $\varphi=0$. It is evident that the morphology of the three products ($\varphi=0.5$, 1 and 1.5) is different from the appearance of their original precursors, possibly ascribed

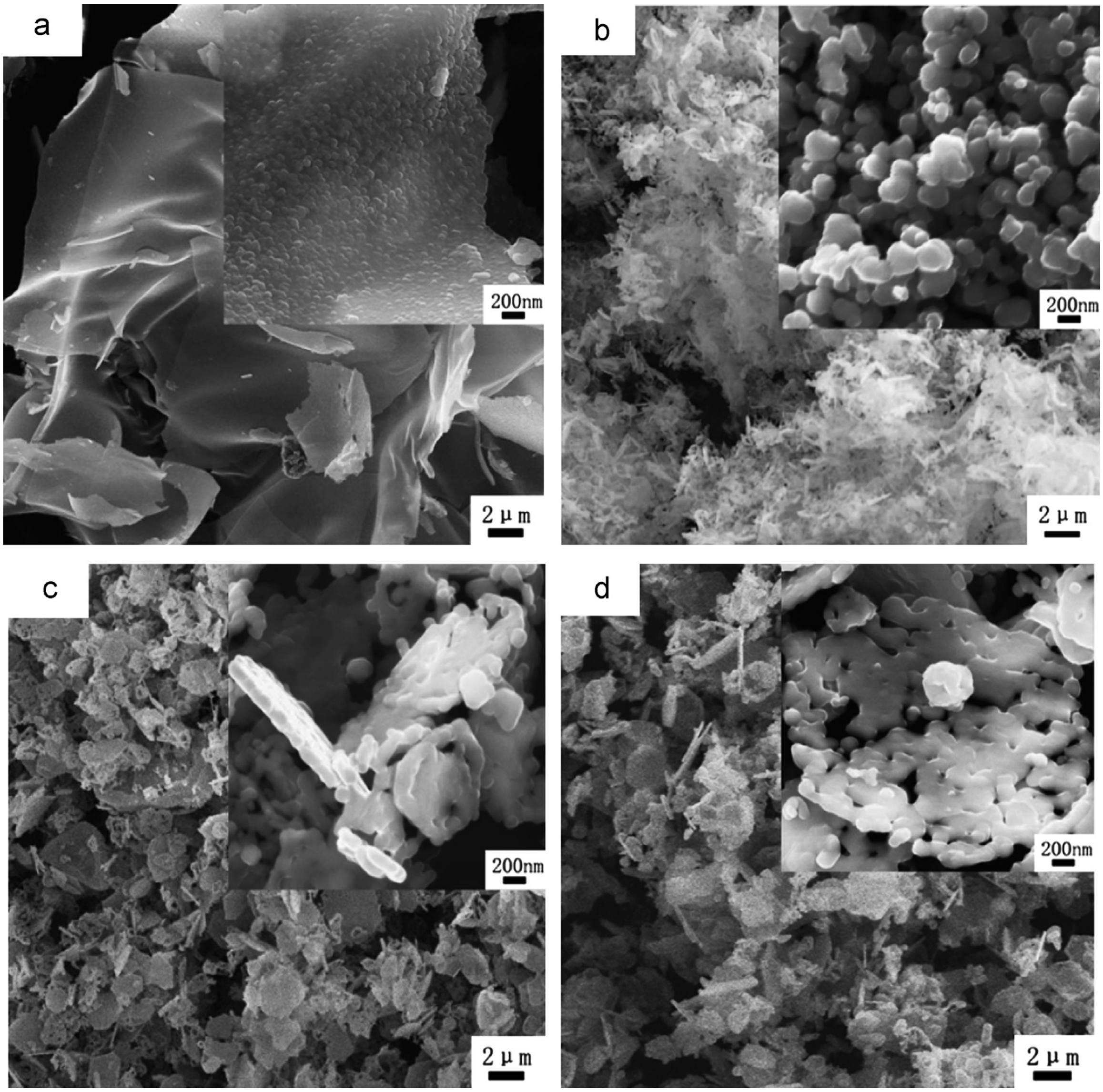

Fig. 5. FESEM images of 1500 °C samples: (a) $\varphi=0$; (b) $\varphi=0.5$; (c) $\varphi=1$; and (d) $\varphi=1.5$.

to the gasification of byproducts during the nitridation process. Furthermore, the SSAs of the four products ($\varphi=0$, 0.5, 1 and 1.5) are calculated to be 21.0, 12.8, 8.7, 6.3 $m^2 g^{-1}$, respectively, indicating that the SSA of the nitridation products is decreasing. The change in trend of the SSA for nitridation products is different from that of the precursors. It is ascribed to the higher driving force for sintering provided by precursors with higher SSA, which coarsen the particles more rapidly during the high temperature calcinations.

3.4. Hard agglomeration analysis of the AlN powders

Fig. 6 shows FESEM images of the fractured surfaces of the AlN green pellet using AlN powders ($\varphi=1.5$) synthesized at 1500 °C. The AlN green pellet has been prepared by pressing the AlN powders at 60 MPa. It is observed from Fig. 6 that the interfaces between the particles of green fracture are very indistinct, and there are no irregular holes visible at the green fracture surface (Fig. 6b). In addition, the original appearance of hexagonal flaky particles vanishes (Fig. 6a). A similar phenomenon can be found in the literature [23], indicating that the uniform and smooth green fracture under pressure results in the powders without the hard agglomeration phenomenon. It demonstrates that AlN powders, synthesized at 1500 °C, are free from any hard agglomeration.

4. Conclusions

Sodium fluoride has a significant effect on the specific surface area, morphology and nitridation reactivities of AlN powders prepared by sodium fluoride-assisted solution combustion synthesis. With the increase of the sodium fluoride content, the morphology of the products change from highly fluffy and porous networks into regular and hexagonal thin flakes. AlN powders synthesized at 1500 °C for 2 h, are free from any hard agglomeration. Moreover, during the nitridation reactivity, the impurity peaks of $NaNO_2$, Na_2CO_3 and $Na_{2.74}Al_{22}O_{38}$ disappear above 1300 °C. The phase-pure AlN has been observed in all

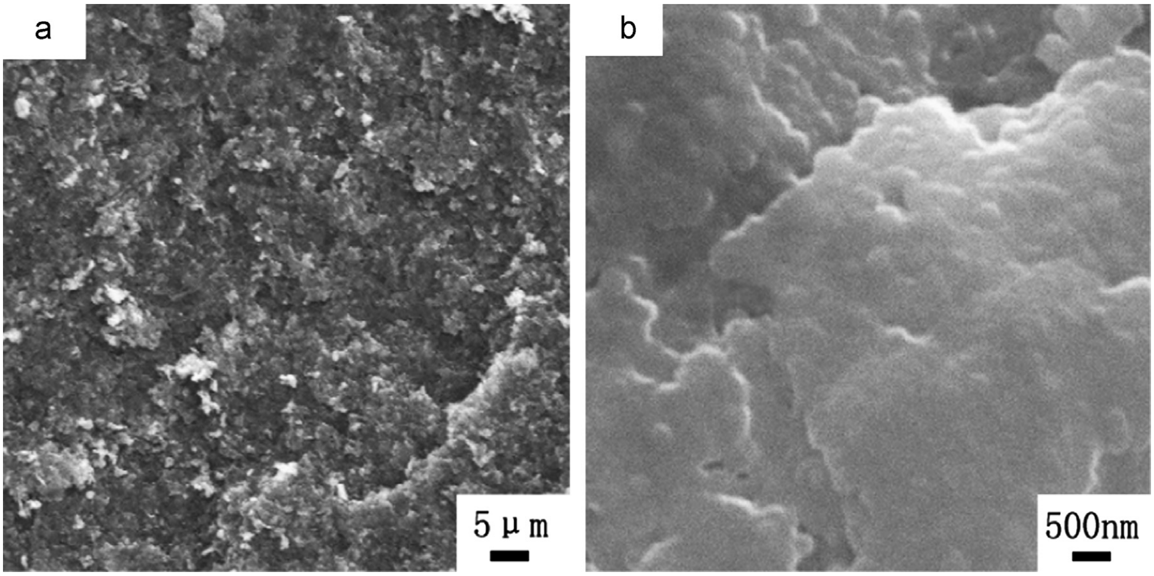

Fig. 6. FESEM images of the fractured surfaces of the AlN green pellet.

products calcined above 1300 °C, and no sodium can be detected in AlN powders by the XRF analysis.

Acknowledgments

This work was supported by the National Natural Science Foundation Program of China (50802006 and 51172017), the Natural Science Foundation Program of Beijing (2102028), and the Fundamental Research Funds for the Central Universities (FRF-TP-11-004A).

References

[1] B. Mussler, Advanced materials & powders, Am. Ceram. Soc. Bull. 79 (2000) 45–47.

[2] T. Jackson, A. Virkar, K. More, R. Dinwiddie, R. Cutler, High-thermal-conductivity aluminum nitride ceramics: the effect of thermodynamic, kinetic, and microstructural factors, J. Am. Ceram. Soc. 80 (6) (1997) 1421–1435.

[3] Y. Kameshima, M. Irie, A. Yasumori, K. Okada, Mechanochemical effect on low temperature synthesis of AlN by direct nitridation method, Solid State Ion. 172 (1) (2004) 185–190.

[4] M. Qin, X. Du, Z. Li, I. Humail, X. Qu, Synthesis of aluminum nitride powder by carbothermal reduction of a combustion synthesis precursor, Mater. Res. Bull. 43 (2008) 2954–2960.

[5] A. Molisani, H. Yoshimura, Low-temperature synthesis of AlN powder with multicomponent additive systems by carbothermal reduction–nitridation method, Mater. Res. Bull. 45 (6) (2010) 733–738.

[6] Y. Sun, J. Li, Y. Tan, L. Zhang, Fabrication of aluminum nitride (AlN) hollow fibers by carbothermal reduction and nitridation of electrospun precursor fibers, J. Alloys Compd. 471 (1) (2009) 400–403.

[7] J. Wagner, C. Mitterer, M. Penoy, C. Michotte, W. Wallgram, M. Kathrein, The effect of deposition temperature on microstructure and properties of thermal CVD TiN coating, Int. J. Refract. Met. Hard Mater. 26 (2) (2008) 120–126.

[8] A. Chu, M. Qin, Rafi-ud-din, B. Jia, H. Lu, X. Qu, Citric acid-assisted combustion-carbothermal synthesis of well-distributed highly sinterable AlN nanopowders, J. Am. Ceram. Soc. 95 (8) (2012) 2510–2515.

[9] A. Chu, M. Qin, Rafi-ud-din, B. Jia, H. Lu, X. He, X. Qu, Effect of aluminum source on the synthesis of AlN powders from combustion synthesis precursors, Mater. Res. Bull. 47 (9) (2012) 2475–2479.

[10] Y. Tang, H. Cong, H. Cheng, Synthesis and properties of one-dimensional aluminum nitride nanostructures, Nano 2 (6) (2007) 307–331.

[11] Q. Zhang, L. Gao, Synthesis of nanocrystalline aluminum nitride by nitridation of δ-Al_2O_3 nanoparticles in flowing ammonia, J. Am. Ceram. Soc. 89 (2) (2006) 415–421.

[12] E. Kroke, L. Loeffler, F. Lange, R. Riedel, Aluminum nitride prepared by nitridation of aluminum oxide precursors, J. Am. Ceram. Soc. 85 (2002) 3117–3119.

[13] T. Suehiro, N. Hirosaki, R. Terao, J. Tatami, T. Meguro, K. Komeya, Synthesis of aluminum nitride nanopowder by gas-reduction–nitridation method, J. Am. Ceram. Soc. 86 (2003) 1046–1048.

[14] T. Yamakawa, J. Tatami, K. Komeya, T. Meguro, Synthesis of AlN powder from $Al(OH)_3$ by reduction–nitridation in a mixture of NH_3–C_3H_8 gas, J. Eur. Ceram. Soc. 26 (2006) 2413–2418.

[15] W. Tseng, C. Lin, Carbothermal reduction and nitridation of aluminum hydroxide, J. Mater. Sci. 31 (1996) 3559–3565.

[16] S. Aruna, A. Mukasyan, Combustion synthesis and nanomaterials, Curr. Opin. Solid State Mater. Sci. 12 (3) (2008) 44–50.

[17] G. Yao, L. Su, X. Xu, J. Xu, Eu: Y_2O_3 nano-phosphor prepared by novel energy-saving solution combustion method, J. Alloys Compd. 462 (1) (2008) 381–385.

[18] A. Chu, M. Qin, Rafi-ud-din, B. Jia, H. Lu, X. Qu, Effect of urea on the size and morphology of AlN nanoparticles synthesized from combustion synthesis Precursors, J. Alloys Compd. 530 (2012) 144–151.

[19] Z. Cao, M. Qin, A. Chu, M. Huang, H. Wu, X. Qu, Glucose-assisted combustion-nitridation synthesis of well-distributed CrN nanoparticles, Mater. Res. Bull. 52 (2014) 74–75.

[20] A. Chu, M. Qin, L. Dan, H. Wu, Z. Cao, X. Qu, Preparation of SiC nanopowder using low-temperature combustion synthesized precursor, Mater. Chem. Phys. 144 (3) (2014) 560–567.

[21] W. Wen, J. Wu, Eruption combustion synthesis of NiO/Ni nanocomposites with enhanced properties for dye-absorption and lithium storage, ACS Appl. Mater. Interfaces 3 (10) (2011) 4112–4119.

[22] C. Manjunatha, B. Nagabhushana, D. Sunitha, H. Nagabhushana, S. Sharma, G. Venkatesh, R. Chakradhar, Effect of NaF flux on microstructure and thermoluminescence properties of Sm^{3+} doped $CdSiO_3$ nanophosphor, J. Lumin. 134 (2013) 432–440.

[23] M. Marinsek, K. Zupan, J. Maeek, Ni–YSZ cermet anodes prepared by citrate/nitrate combustion synthesis, J. Power Sources 106 (2002) 178–188.